Available online at www.sciencedirect.com
ScienceDirect
International Journal of Heat and Mass Transfer 50 (2007) 3471–3480
International Journal of HEAT and MASS TRANSFER
www.elsevier.com/locate/ijhmt

# Laminar flow and heat transfer in a periodic trapezoidal channel with semi-circular cross-section

Paul. E. Geyer, David F. Fletcher *, Brian S. Haynes

*School of Chemical and Biomolecular Engineering, University of Sydney, NSW 2006, Australia*

Received 8 September 2006; received in revised form 10 January 2007
Available online 5 April 2007

**Abstract**

Computational fluid dynamics (CFD) has been used to study fully developed laminar flow and heat transfer behaviour in periodic trapezoidal channels with a semi-circular cross-section. The trapezoidal elements are characterised by their wavelength ($2L$), channel diameter ($d$), radius of curvature of bends ($R_c$), the amplitude ($2A$) and the length of the straight section ($B$) with results reported for Reynolds numbers ($Re$) up to 400, as well as for a range of geometric configurations ($0.525 \leqslant \frac{R_c}{d} \leqslant 1.3$, $3.6 \leqslant \frac{L}{d} \leqslant 12$, $0.17 \leqslant \frac{B}{L} \leqslant 1$, $0.125 \leqslant \frac{A}{L} \leqslant 1$) at $Re = 200$. This generic geometry takes a variety of shapes with limiting forms of a regular square serpentine ($B = 2A = L$) and a zig-zag or saw-tooth ($B \to 0$). The flow in these channels is characterised by the formation of Dean vortices following each bend. As the Reynolds number is increased, stronger vortical flow patterns emerge and these vortices lead to efficient fluid mixing and high rates of heat transfer.

Constant wall heat flux (H2), constant axial heat flux with peripherally constant temperature (H1) and constant wall temperature (T) boundary conditions are examined for a fluid with a Prandtl number of 6.13. Higher rates of heat transfer with relatively small pressure loss penalty are found relative to fully developed flow in a straight pipe, with heat transfer enhancements of up to four at the highest Reynolds number.

In addition to presenting channel enhancements the stackability of channels on a plate is considered. The concepts of area enhancement (based solely on geometric factors) and heat transfer intensification, the product of the heat transfer enhancement and the area enhancement, are introduced and used to compare different geometrical configurations. The swept zig-zag pathway provided the greatest intensification of heat transfer in a multi-channel plate structure.


*Keywords:* Trapezoidal path; Heat transfer; CFD; Fluid flow; Enhancement; Intensification

## 1. Introduction

Laminar flow heat transfer and means by which it can be enhanced has become a subject of increased interest following the recent drive towards miniaturisation of heat transfer devices for a wide range of applications, including electronics cooling, solar heat collectors, micro-chemical processing and compact heat exchanger design. This need has driven a considerable number of computational studies into laminar flow and forced heat transfer in a variety of channel geometries, including those with circular and circular sector [1], triangular [2], rhombic [3], trapezoidal [4] and semi-elliptic [5] cross-sections. Even with a complex channel shape there is still the need to disrupt the thermal boundary layer beyond the entrance region in order to enhance heat transfer. For these application the Reynolds number is too low to benefit from turbulence, so that geometrical effects, such as the use of sinusoidal channels [6,7] or corrugated channels [8], insertion of twisted tapes [9,10], introduction of ribs [11] or the creation of flow instabilities, such as Dean vortices [12–14] have all been used to enhance heat transfer. Recently, a CFD model has been linked to a

* Corresponding author. Tel.: +61 2 93514147; fax: +61 2 93512854.
*E-mail address:* d.fletcher@usyd.edu.au (D.F. Fletcher).

0017-9310/$ - see front matter © 2007 Elsevier Ltd. All rights reserved.
doi:10.1016/j.ijheatmasstransfer.2007.01.050

**Nomenclature**

| | |
|---|---|
| $A$ | trapezoidal amplitude (no subscripts) (m) |
| $A$ | area ($m^2$) |
| $B$ | length of the short side of the trapezoid (m) |
| $d$ | diameter of semi-circular channel (m) |
| $e$ | dimensionless enhancement/penalty factor |
| $f$ | Fanning friction factor |
| $g$ | diagonal distance used in Appendix A, Scheme I (m) |
| $h$ | heat transfer coefficient ($W\,m^{-2}\,K^{-1}$) |
| $i$ | heat transfer intensification |
| $k$ | thermal conductivity ($W\,m^{-1}\,K^{-1}$) |
| $L$ | trapezoidal unit half-wavelength (m) |
| len | length used in Appendix A, Scheme II (m) |
| $Nu$ | Nusselt number |
| $P$ | channel cross-section perimeter length (m) |
| $\Delta P$ | channel pressure-drop (Pa) |
| $Pr$ | Prandtl number |
| $R_c$ | radius of curvature (m) |
| $Re$ | Reynolds number |
| $S$ | channel axial path length (m) |
| $t$ | minimum wall thickness between stacked channels (m) |
| $u$ | $x$-component velocity ($m\,s^{-1}$) |
| $v$ | $y$-component velocity ($m\,s^{-1}$) |
| $x$ | $x$-coordinate (m) |
| $y$ | $y$-coordinate (m) |

*Greek symbols*

| | |
|---|---|
| $\alpha$ | angle used in Appendix A, Scheme I |
| $\delta$ | channel pitch (m) |
| $\eta$ | enhancement efficiency (dimensionless) |
| $\omega$ | vorticity ($s^{-1}$) |

*Subscripts*

| | |
|---|---|
| A | plate area based quantity |
| app | apparent |
| channel | channel property |
| f | pressure-drop penalty factor |
| $Nu$ | heat transfer enhancement factor |
| plate | theoretical heat exchanger plate |
| straight | straight channel |

structural optimisation routine in order to determine the two-dimensional channel path that gives the greatest heat transfer augmentation for a given increase in pumping power [15].

As noted above, enhancement of heat transfer in laminar flows may be achieved through making the flow follow a tortuous path. However, much of the previous work has been concerned with flow in helical coils, which is not directly relevant to the design of plate type heat exchangers. We have recently examined fully developed laminar flow and heat transfer in serpentine passages of various geometrical configurations and cross-sections, and reported the benefits of using such passages to obtain high rates of heat transfer with comparatively low friction factors [16–19]. The establishment of secondary flows in the form of Dean vortices at the serpentine bends is responsible for transverse convection that brings fluid from the centreline of the duct path to the wall. There is very little pressure loss in creating these flows and the heat transfer for water flows may be enhanced by a factor of up to three, relative to the pressure-drop penalty.

While the serpentine passage represents an interesting model flow path, it is not ideal for application in plate structures because the passages cannot be placed close together, i.e. they have poor stackability and make poor use of the available plate area. A channel with a much higher packing density, or 'stackability', which maintains the system of alternating bends seen in the serpentine channels, is one with a trapezoidal axial path, shown schematically in Fig. 1. In this paper, we report a computational

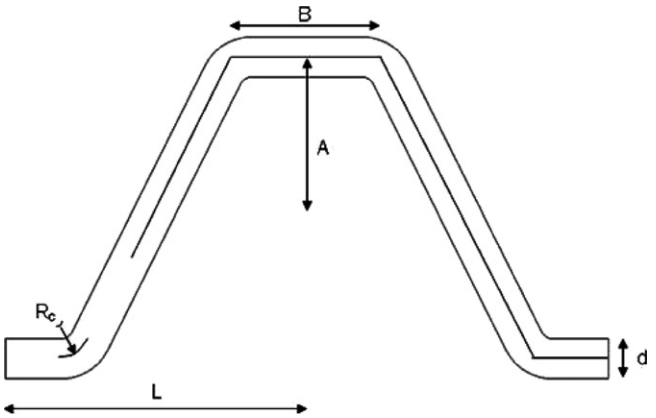


Fig. 1. The general dimensions in the trapezoidal unit. The length of the top run, $B$, is defined as the distance between intersections of the centre lines of the top and the angled sides.

fluid dynamics analysis of the laminar thermohydraulics of channels following a trapezoidal path, ranging from the regular square serpentine ($B = 2A = L$ in Fig. 1) to a zig-zag or saw-tooth ($B \to 0$). This important class of channel paths appears not to have been studied previously.

In addition to characterising the heat transfer enhancement for standalone trapezoidal channels, we also bridge the gap between the characteristics of single channel flow and the performance of heat exchanger plates that incorporate such channels, taking into account the channel density achievable in a plate structure. In keeping with the focus here on plate structures, the channels in this study have a semi-circular cross-section, with the chord of the semi-

circle lying in the plane of the plate surface. This cross-section choice was made because it is characteristic of the channel shape obtained by etching.

## 2. Computational methods

The trapezoidal passages shown in Fig. 1 are defined by sweeping a semi-circle along the path, with the flat face of the semi-circle lying in the swept plane. The geometry is fully characterised by the unit half-length, $L$; the diameter of the semi-circular cross-section, $d$; the radius of curvature of the bends, $R_c$; the half-height of the trapezoid, $A$; and the length of straight run, $B$. We non-dimensionalise the geometry using the ratios $L/d$; $R_c/d$; $A/L$; and $B/L$. These parameters are varied over the ranges given in the following equation:

$$0.525 \leqslant \frac{R_c}{d} \leqslant 1.3, \tag{1a}$$

$$3.6 \leqslant \frac{L}{d} \leqslant 12, \tag{1b}$$

$$0.17 \leqslant \frac{B}{L} \leqslant 1, \tag{1c}$$

$$0.125 \leqslant \frac{A}{L} \leqslant 1. \tag{1d}$$

Note that the lower limit of $B/L$ is set by the constraint that there is a positive radius of curvature at the inside of the bends: The case $B/L = 1$ is precisely the serpentine system, studied previously. The value $A/L = 0$ corresponds to the limiting case of a straight duct, and the value $R_c/d = 0.5$ corresponds to a sharp corner (zero radius of curvature) at the inside of any bend.

Steady state flow and heat transfer solutions have been found for fully-developed laminar flow for Reynolds numbers up to 400 using ANSYS CFX10, via the method detailed in Rosaguti et al. [16], for a fluid with constant properties and a Prandtl number $Pr = 6.13$ (water). ANSYS CFX10 is a finite-volume code that solves the Navier–Stokes equations using a coupled solver, which treats the pressure–velocity coupling via a modified Rhie–Chow procedure. All the calculations are carried out using a second-order bounded differencing scheme for the convective terms. Fluid velocities and temperatures were wrapped from the outlet to the inlet of a system consisting of three primary units in series. Three units were employed because the velocity and temperature gradients are not wrapped and the flow is therefore not truly fully developed in the first and third sections. The results from the middle section do represent fully developed periodic flow [16] and these are reported here. The system was regarded as having reached a converged state once the domain imbalances and scaled residuals for the mass, momentum and energy equations had fallen below $1 \times 10^{-5}$. The Reynolds number study was limited to $Re \leqslant 400$, as tests at a Reynolds number of 450 revealed the onset of unsteady flow.

A structured mesh was used in the discretisation of the system. The cross-sectional mesh (2097 surface elements),

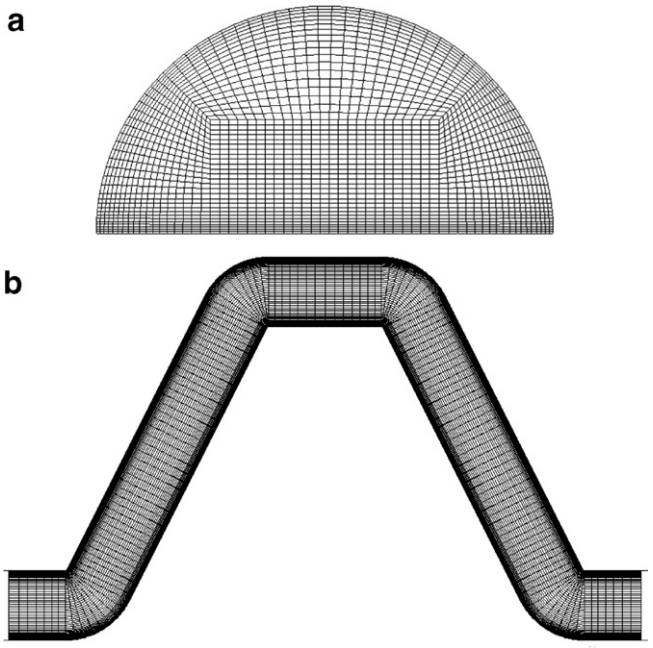


Fig. 2. Schematic of (a) the cross-sectional and (b) the longitudinal mesh densities used in calculations for the base case ($R_c/d = 0.8$, $L/d = 4.5$, $B/L = 0.5$, $A/L = 0.5$).

shown in Fig. 2a, was previously shown to provide grid-independent solutions [17]. The longitudinal mesh density, shown in Fig. 2b, was set such that the node groups were distributed relatively evenly along the flow axis, with a slightly higher density towards the bends. Serpentine models used in previous work [18] contained approximately 10 axial element groups along a section of channel of length $d$. This longitudinal mesh density was shown to give grid independent solutions. It has therefore been used as a guide to determine the longitudinal density here, resulting in 120–160 element groups along the flow axis of each channel. In order to construct the meshes with the desired geometric properties the dimension $L$ was set to a value of 9 mm and all other dimensions were obtained from the chosen non-dimensional parameters.

Heat transfer (wall heat transfer coefficients) and pressure-drop data were obtained from the converged solution, as previously described in Geyer et al. [18]. The results are expressed as Nusselt numbers (peripherally averaged at a cross-section and averaged over the whole test section) and mean Fanning friction factors, $f$ (calculated on the basis of the actual path length of the section). Here, in Eqs. (2) and (3), we report only normalised values, relative to the values of $Nu$ and $f$ pertaining to fully-developed laminar flows in straight passages with the same semi-circular cross-section and the same overall path length:

$$e_{Nu} = \frac{Nu_{\text{channel}}}{Nu_{\text{straight}}} \tag{2}$$

$$e_f = \frac{\Delta P_{\text{channel}}/S}{\Delta P_{\text{straight}}/S} = \frac{f_{\text{channel}}}{f_{\text{straight}}} \tag{3}$$

Table 1
A comparison of results of the present simulations with literature values for heat transfer and pressure-drop parameters for straight semi-circular ducts

| | Literature ([20]) | Current simulations | Percentage difference (%) |
|---|---|---|---|
| $f \cdot Re$ | 15.767 | 15.788 | 0.133 |
| $Nu_{straight,H1}$ | 4.089 | 4.0897 | 0.018 |
| $Nu_{straight,H2}$ | 2.923 | 2.925 | 0.068 |
| $Nu_{straight,T}$ | 3.323[a] | 3.326 | 0.090 |

[a] This value was taken from [17].

The values of $Nu_{straight}$ and $f_{straight}$ used are given in Table 1. The table also contains results from simulations performed for straight ducts in order to validate the computational model used here. Excellent agreement with published data is obtained. There is a minor difference between the Nusselt number produced for the T boundary condition between this and our previous work, since here we have used grid sizes that can be used in practical geometries whereas the value presented in [17] was obtained using an extremely fine mesh to give a benchmark value.

## 3. Results for a single trapezoidal channel

Results have been obtained for laminar flows ($0 < Re < 400$) with constant fluid properties ($Pr = 6.13$). The boundary conditions studied were constant wall heat flux (both the H1 and H2 boundary conditions of Shah and London [20]) and constant wall temperature (the T boundary condition).

Fig. 3 shows the effect of fluid Reynolds number ($0 < Re < 400$) on the relative pressure-drop penalty and the enhancement of heat transfer in the base-case geometry depicted in Fig. 2. The heat-transfer enhancements are only of the order of 20% at $Re = 50$ but rise to $e_{Nu} \sim 4$ at $Re = 400$. The enhancements for the T and H2 boundary conditions are virtually identical and slightly larger than for the H1 boundary condition, similar to the behaviour

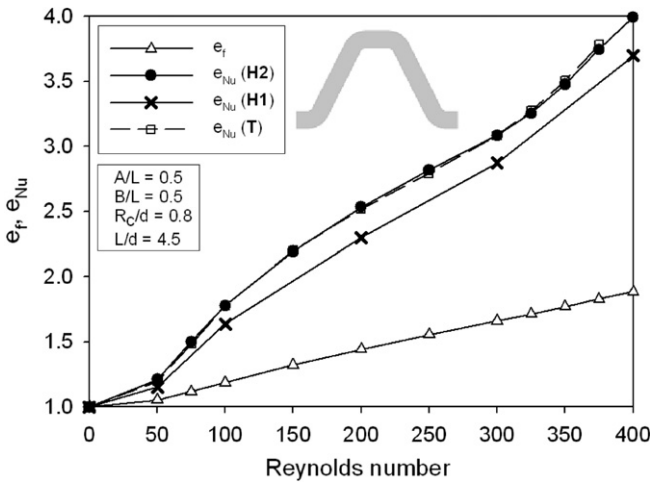


Fig. 3. Heat transfer enhancement and pressure-drop penalty as a function of Reynolds number for the base case geometry shown in Fig. 2.

observed in the serpentine system [21]. The enhancement of the heat transfer significantly exceeds the relative pressure-drop penalty throughout the range studied.

Fig. 4 presents the results obtained for parametric variations about the base case geometry at $Re = 200$. We calculated these results only for the H2 boundary conditions because of the vastly greater computational effort needed for the H1 condition [21] but the general trends shown can also be expected to apply for the H1 condition. Results for the T boundary condition have been omitted as they are very similar to the H2 results, as in Fig. 3. Increasing $R_c/d$ (Fig. 4a), making the corners more rounded, slightly reduces the pressure-drop and also leads to a small reduction in the heat transfer enhancement. The effect of $L/d$ (Fig. 4b) is more complex, with a weak maximum in the heat transfer enhancement occurring at $L/d \sim 5$; the pressure-drop penalty is greatest at low $L/d$ and decreases monotonically as that parameter is increased. In the limit, as $L/d \to \infty$, both $e_{Nu}$ and $e_f$ will approach unity as the effect of the corners becomes negligible compared with that of the straight runs. These results for variation of the $R_c/d$ and $L/d$ parameters are qualitatively similar to those for the square serpentine presented previously [16,17].

Fig. 4c shows the effect of varying the length of the short side of the trapezoid, $B$. While the shape of the duct path changes significantly, from zig-zag at $B/L \sim 0$ to square serpentine at $B/L = 1$, there is remarkably little effect on the results for heat transfer enhancement and pressure-drop penalty. The height of the trapezoid, parameterised as $A/L$, has a significant effect on the results only at small values of $A/L$, as shown in Fig. 4d. The value of $A/L = 0$ corresponds to straight duct flow – enhancements are significant even for small wave heights ($A/L = 0.13$) but much of the effect of varying $A/L$ is achieved already at $A/L = 0.25$, beyond which there is only a slight increase in heat transfer enhancement, albeit with slightly reduced pressure-drop penalty.

Analysis of local flow patterns and heat transfer enhancements reveals the mechanisms responsible for the enhancements presented above. We illustrate this with reference to the effect of varying the parameter $A/L$, as shown in Fig. 4d. Fig. 5 shows peripherally-averaged heat transfer enhancement for various values of $A/L$ – the trapezoidal section is broken into its component parts (straight runs and bends) in order to show the effects of the parametric changes more clearly. At low $A/L$, enhancement is relatively weak and uniformly distributed along the path. As $A/L$ increases, the bend angle and the arc length of the bend (at constant radius of curvature) increase, leading to the development of more pronounced Dean vortices. As previously discussed in detail [18], these vortices promote fluid mixing in the bends and, depending on whether the bend direction reinforces or cancels the direction of the previous bend, give rise to higher heat transfer coefficients in and beyond the corner. At the same time as $A/L$ increases, the length of the sloped sides of the trapezoidal path increases so there is a greater tendency for the Dean

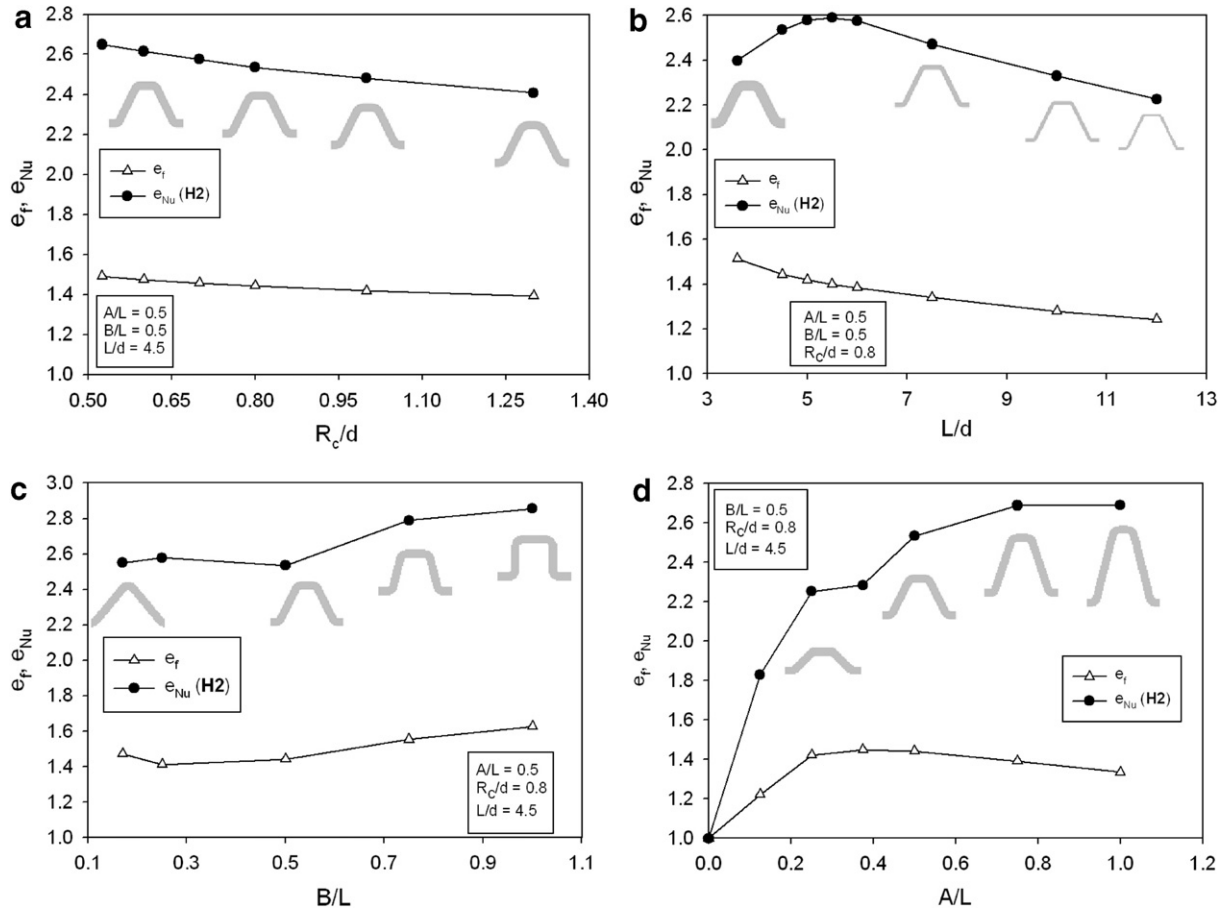


Fig. 4. Heat transfer enhancements and relative pressure-drop penalties at $Re = 200$ for the base case geometry (Fig. 2) with perturbations in: (a) $R_c/d$; (b) $L/d$; (c) $B/L$; and (d) $A/L$.

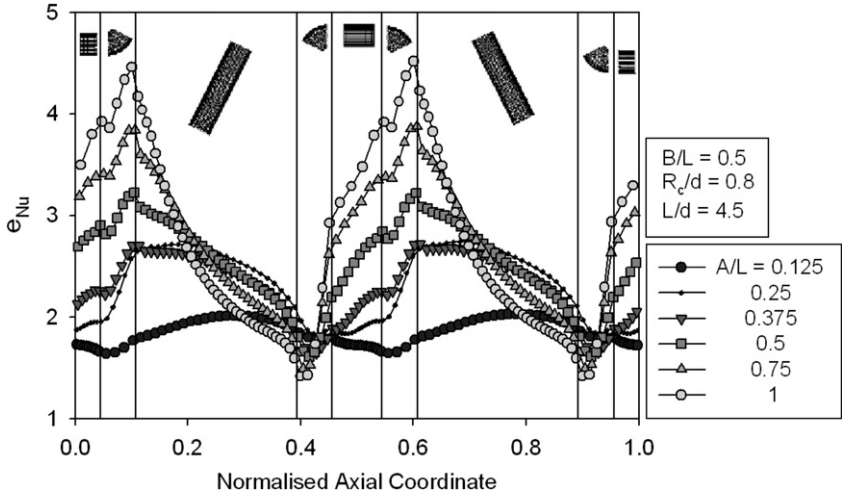


Fig. 5. Peripherally-averaged heat transfer enhancements at $Re = 200$ for the base case geometry with different values of $A/L$. Note that the curves have been standardised using the base case ($A/L = 0.5$), so that bend entrance/exits all occur at the same point.

vortices to dissipate, with the result that the local heat transfer enhancement is also increasingly lost along these sides.

The plots in Fig. 5 also show that there is an increase in heat transfer enhancement along the length of the horizontal section of channel between two bends, an effect that becomes more marked at higher $A/L$. This points to the Dean vortices becoming more pronounced further along the horizontal length, the opposite of what is expected in a straight section of channel. We believe this is because

the section of channel between the start of one bend and the end of the next behaves more like one continuous bend at higher $A/L$, with the longer bend arc length at higher $A/L$ resulting in a decrease in the length of horizontal section (at constant $B/L$).

The effect of the more pronounced vortices in the horizontal sections is explored at a local level in Fig. 6. These plots show the influence of fluid shear (mixing) on the temperature distribution in the fluid. The degree of shear is given by the magnitude of the tangential vorticity, which, on an $x$–$y$ plane, is given by:

$$|\omega| = \sqrt{\left(\frac{\partial v}{\partial x} - \frac{\partial u}{\partial y}\right)^2}. \tag{4}$$

The vorticity plots point to the presence of two vortex cores in the fluid, and thinner boundary layers (but with a higher vorticity) along the adjacent channel walls. There is both an increase in the extent and magnitude of the high-shear zones as $A/L$ increases and this has a marked effect on the thermal boundary layer of the fluid. As Fig. 6a shows, at low $A/L$, the thermal boundary layer is quite pronounced, with a well-defined temperature profile, and a large zone of hot fluid along the wall. As $A/L$ increases, the boundary layer thins, until at $A/L = 1$ (Fig. 6d), it is fully disrupted and a large proportion of the wall is in close contact with cold fluid.

Fig. 4d shows that there is a local maximum in heat transfer enhancement between $A/L = 0.25$ and $A/L = 0.375$. The equivalent axial enhancement plots in Fig. 5 suggest a transition of secondary flow schemes between these values. Both cases display nearly the same maximum enhancement coming out of the reinforcing bends, but the rate of decrease of enhancement in the following straight section is lower at the lower value of $A/L$ (=0.25) because the vortices survive longer. The greater loss of enhancement here at $A/L = 0.375$ is offset by the development of stronger vortices in the top of the trapezoid, as previously discussed.

## 4. Considerations for plate design

A rudimentary method of comparing the heat transfer enhancement and the pressure-drop penalty used in previous studies [8,18,22] is given by the enhancement efficiency defined by:

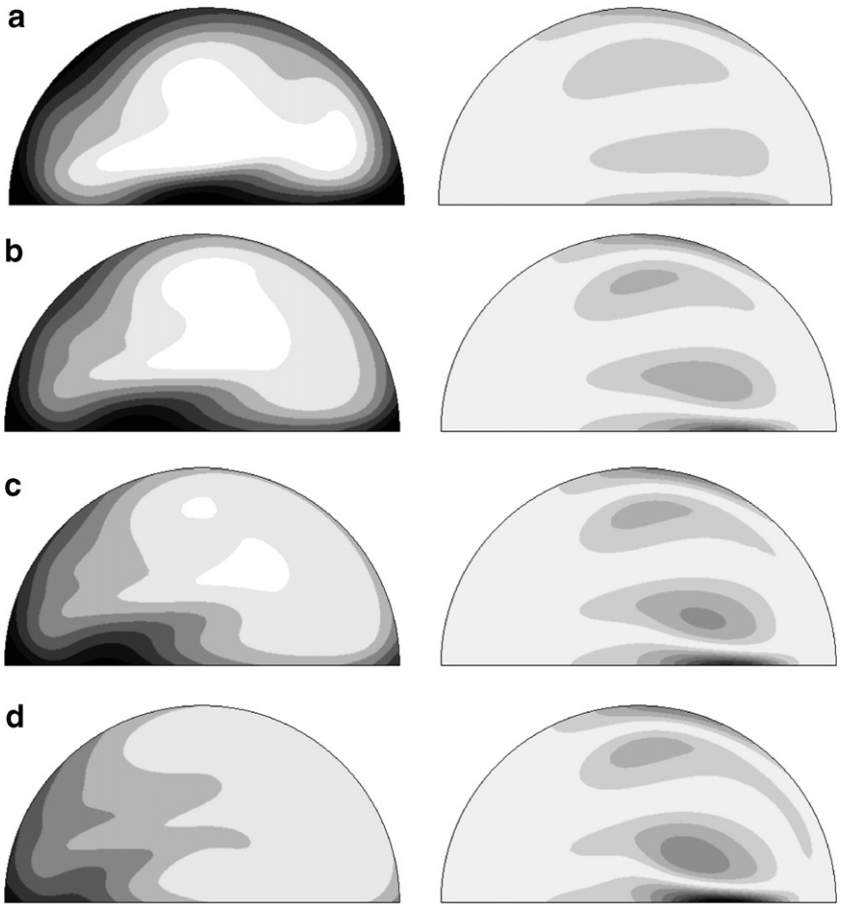


Fig. 6. Fluid temperature (left) and vorticity (right) plots for selected systems shown in Fig. 5: (a) $A/L = 0.25$; (b) $A/L = 0.375$; (c) $A/L = 0.5$; (d) $A/L = 1$. For the temperature contours, darker shading indicates hotter fluid (temperature range 303–343 K). For the vorticity contours, darker shading indicates higher vorticity (vorticity range 0–2500 $s^{-1}$). Snapshots taken at the inlet of the second unit. The fluid is flowing into the page.

$$\eta = \frac{e_{Nu}}{e_f}. \tag{5}$$

This efficiency measure is really only suited to comparing single channels of the same length. It does not give any indication of how effectively the overall plate area in an exchanger is utilised when tortuous channels, such as with serpentine or trapezoidal paths, are introduced onto the plate surface. Here we consider a broader concept of efficiency that includes not only the thermohydraulics of the channel but also the packing of channels onto a plate.

A tortuous path serves to enhance the heat transfer relative to the performance obtainable with straight passages. However, the non-straight passage occupies more area on a plate and it is important to compare not only the heat transfer coefficient but also the area of plate that is required, in order to assess the degree of intensification that can be achieved. We consider the situation that generally arises in microchannel heat transfer in metallic systems where the thermal resistance of the walls is negligible. The primary heat transfer surface is then the channel wall area, while the system size is essentially determined by the plate area. The apparent heat transfer coefficient based on the plate area is then given by:

$$h_{app} = h\frac{A_{channel}}{A_{plate}}, \tag{6}$$

where $A_{channel}$ is the total wall area of all the channels on the plate.

Considering a length of plate with straight channels of width $d$, separated by a wall of thickness $t$, the apparent area density is given by:

$$(A_{channel}/A_{plate})_{straight} = \frac{P}{d+t}, \tag{7}$$

where $P$ is the perimeter of the channel cross-section.

The apparent area density of tortuous channel paths depends very much on the pathway – i.e. on how closely adjacent channels can be nested – as well as on the minimum wall thickness required between channels, usually determined by manufacturing and structural integrity requirements. The calculation of the channel pitch ($\delta$, the distance between a given point on one channel and the location of the same point on the next channel on the plate) is described in detail in Appendix A for the swept trapezoidal pathway.

Once the pitch is known, the apparent area density for the particular channel path is given by:

$$(A_{channel}/A_{plate}) = \frac{P \cdot S}{2L\delta}, \tag{8}$$

where $S$ is the path length of one unit of the repeating geometry which has wavelength $2L$.

The heat transfer intensification relative to straight passages is given in:

$$i_A = \frac{h_{app}}{h_{app}|_{straight}} = \left[\frac{h}{h_{straight}}\right] \cdot \left[\frac{(A_{channel}/A_{plate})}{(A_{channel}/A_{plate})_{straight}}\right] = e_{Nu} \cdot e_A. \tag{9}$$

The area enhancement ($e_A$ – the ratio of area densities in Eqs. (7) and (8)) simplifies to:

$$e_A = \frac{S(d+t)}{2L\delta}. \tag{10}$$

We use the nomenclature "area enhancement" only for consistency with our definitions of $e_{Nu}$ and $e_f$ – in fact the area enhancement is invariably $\leqslant 1$. For reasonably stackable geometries (Scheme I in Appendix A) Eq. (10) can be further simplified:

$$e_A = \frac{S \cdot \cos\alpha}{2L}, \tag{11}$$

where $\alpha$ is the angle of deviation of the side of the trapezoid from the horizontal (see Appendix A). This shows that the area enhancement is independent of wall thickness for stackable geometries. For values of $\alpha$ approaching 90°, the swept geometry actually stacks better than implied by Eq. (11) because of the differing radii of curvature on the inner and outer bends of the trapezoid. Ultimately, the area density cannot fall below the value obtained for no overlap of the channels – this situation is described in Scheme II in Appendix A.

Fig. 7 shows the plots of area enhancement and intensification for the systems used in the study of parametric variations (Fig. 4). As shown in Figs. 7a and b, $R_c/d$ and $L/d$ have very little effect on the area enhancement. This is because in these cases, the enhancement depends only on the ratio $S/L$ (Eq. (11) being valid for all variations in $R_c/d$ and $L/d$) and this ratio changes by <3%. The variations in heat transfer intensification are therefore due only to the changes in heat transfer enhancement discussed previously.

Variations in $B/L$ have a significant impact on area enhancement and intensification as shown in Fig. 7c. From the zig-zag geometry at $B/L \sim 0$, to the serpentine geometry at $B/L = 1$, the area enhancement declines ~50% because the angle $\alpha$ increases and so therefore does the channel pitch $\delta$. Since the heat transfer enhancement over this range of geometries is nearly constant, the observed heat transfer intensification declines significantly although the square serpentine geometry is still better than straight passages ($i_A \sim 1.3$).

Increases in $A/L$ also cause $\alpha$ to increase, with a loss of area utilisation, as shown in Fig. 7d. The marked heat-transfer enhancement at low $A/L$ still provides significant area intensification but this effect weakens at high $A/L$ due to the loss of area.

It should be noted that all of the geometries considered above are swept and have area densities less than that which could be achieved using straight passages with the same channel diameter and minimum wall thickness. Only a perfectly stackable geometry will have an area utilisation

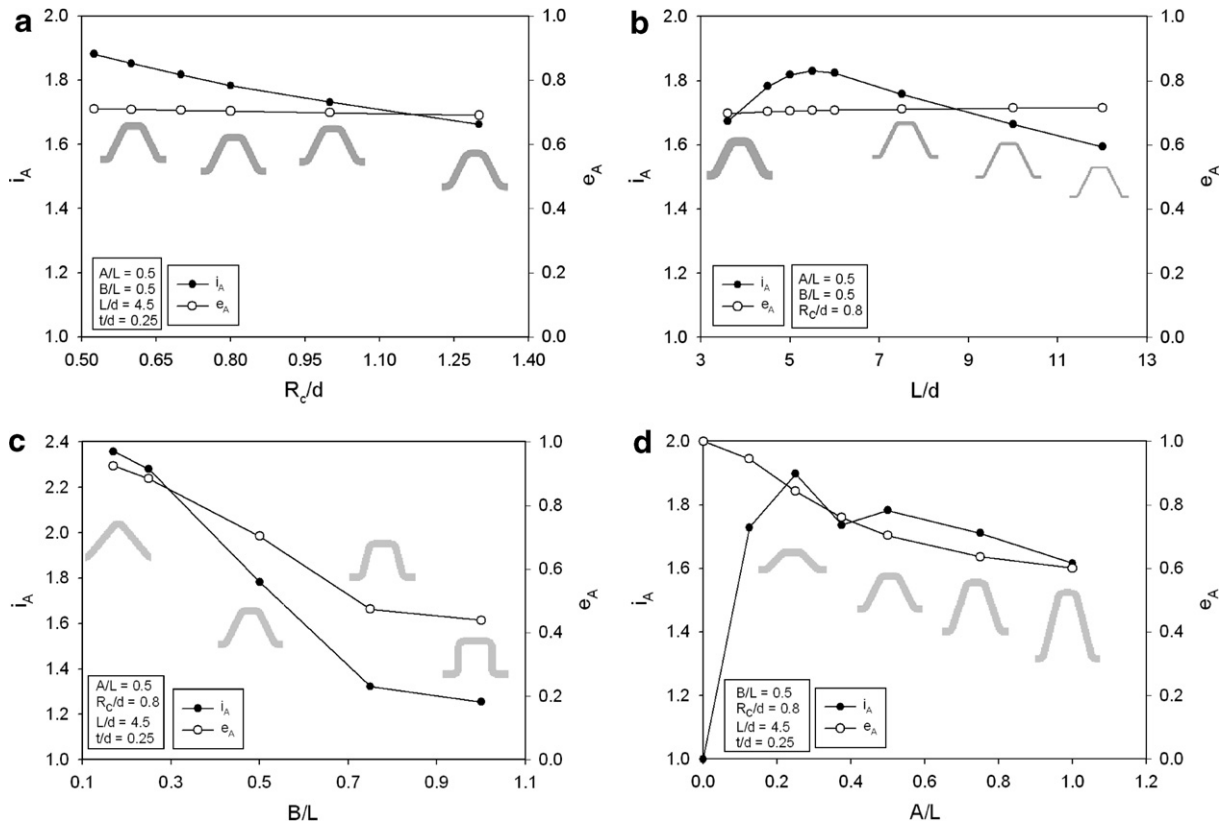


Fig. 7. Heat transfer intensification ($i_A$) and area enhancement ($e_A$) at $Re = 200$ for the base case geometry (Fig. 2) with perturbations in: (a) $R_c/d$; (b) $L/d$; (c) $B/L$; and (d) $A/L$. Note that in case (b) for the $L/d$ variation the value of $t$ has been held fixed at the value used for the base case calculation.

Table 2
Area enhancements for a number of geometries

| Geometry | Area enhancement |
|---|---|
| Perfect saw-tooth | 1 |
| $B/L = 0.17$ | 0.9247 |
| Base case ($B/L = 0.5$) | 0.7031 |
| Serpentine ($B/L = 1$) | 0.4391 |

In all cases, amplitude $A = 0.5L$, and period $= 2L$.

the same as that of the equivalent straight passage. An example of one such geometry is the sharp zig-zag (although this is not a swept geometry). In this case $\delta = S(d + t)/2L$, which when substituted in Eq. (10) gives an $e_A$ value of unity. Typical area enhancements for various geometries studied here are summarised in Table 2.

## 5. Conclusions

CFD simulations of laminar flow heat transfer in repeated trapezoidal channels of semi-circular cross-section have been performed for a wide range of geometric parameters that change the channel shape from a zig-zag to a serpentine. Simulations covered the Reynolds number range 5–400 for a fluid with a Prandtl number of 6.13 and were carried out for the H1, H2 and T thermal boundary conditions. In general, it was possible to obtain significant heat transfer enhancement for a very modest increase in pressure loss, with surprisingly little effect of changing from a zig-zag (with rounded corners) to a serpentine.

Channels with a trapezoidal axial path configuration are well suited for use in compact plate heat exchangers, as their shape generally allows rows of them to be stacked close together. As the angle of the bends approaches 90° the stackability decreases rapidly.

The concept of area efficiency is introduced to define how well channels can be stacked onto a plate as a function of both their shape and the required separation distance. This, when multiplied by the relative enhancement of the mean heat transfer efficiency, gives a heat transfer intensification factor which provides a measure of the efficiency of using a plate with the given channel path, relative to equivalent straight channels.

The swept zig-zag pathway provides the greatest heat transfer intensification of all the paths investigated in this work.

## Acknowledgements

The authors acknowledge the Heatric division of Meggitt (UK) Ltd. for their support of this work. The Australian Research Council provided an Australian Postgraduate Award Industry (APAI) scholarship for Paul Geyer.

## Appendix A. Calculation of channel pitch

There are two schemes to determine channel pitch. Scheme I is always used first.

*Scheme I*

This method is detailed graphically in Fig. 8a. The angle $\alpha$ is easily calculated as the arctangent of $2A/(L-B)$. Given this new angle, and the fixed quantity $(d+t)$, the distance $g$ may be determined using:

$$g = \frac{(d+t)(2A)}{(L-B)}. \tag{A1}$$

If the length $g$ is greater than the length of the straight diagonal section (which can occur at low $L/d$ or low $\alpha$), the configuration in Fig. 8b is used (Scheme II). If it is not, then $\delta$ may be readily derived using:

$$\delta = \frac{(d+t)}{\cos\alpha}. \tag{A2}$$

*Scheme II*

This method (detailed graphically in Fig. 8b) must be used if the length $g$ is greater than the diagonal length because Scheme I does not take bend curvature into account. The derived value of $\delta$ would be too large, and the actual wall thickness would be larger than necessary. The lengths $x_2$ and $z_2$ are given in:

$$x_2 = 2(A - R_c), \tag{A3}$$

$$z_2 = L - 0.5 \times \text{len}_{\text{straight,horizontal}}, \tag{A4}$$

where $\text{len}_{\text{straight,horizontal}}$ is the length of the horizontal section between two bends.

Once $x_2$ and $z_2$ are calculated the length $x_3$ is easily derived using:

$$x_3 = \sqrt{(t + 2R_c + d)^2 - (z_2)^2}. \tag{A5}$$

The overall channel pitch is simply $\delta = x_2 + x_3$.

For all the geometries studied, only those with $B/L = 0.75$ and $B/L = 1$ required the use of this calculation scheme.

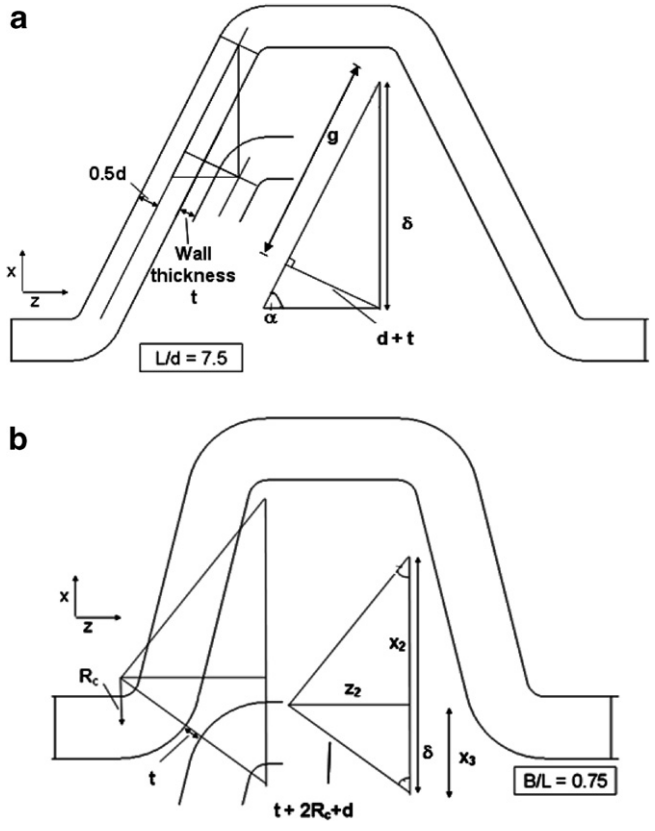


Fig. 8. The two configurations used to determine the separation distance between two successive rows of channels. Configuration (a) is used initially, while configuration (b) is used only if the length $g$ is greater than the length of the straight diagonal.

## References

[1] Q.M. Lei, A.C. Trupp, Forced convection of thermally developing laminar flow in circular sector ducts, Int. J. Heat Mass Transfer 33 (8) (1990) 1675–1683.
[2] S. Chen, T.L. Chan, C.W. Leung, B. Yu, Numerical prediction of laminar forced convection in triangular ducts with unstructured triangular grids, Numer. Heat Transfer A 38 (2000) 209–224.
[3] Y.-M. Lee, P.-C. Lee, Heat transfer coefficients of laminar flow in a rhombic duct with constant wall temperature, Numer. Heat Transfer A 42 (2002) 285–296.
[4] B. Farhanieh, B. Sunden, Three-dimensional laminar flow and heat transfer in the entrance region of trapezoidal ducts, Int. J. Numer. Meth. Fluids 13 (1991) 537–556.
[5] K. Velusamy, V.K. Garg, G. Vaidyanathan, Fully developed flow and heat transfer in semi-elliptical ducts, Inter. J. Heat Fluid Flow 16 (1995) 145–152.
[6] J. Zhang, J. Kundu, R.M. Manglik, Effect of fin waviness and spacing on the lateral vortex structure and laminar heat transfer in wavy-plate-fin cores, Int. J. Heat Mass Transfer 47 (2004) 1719–1730.
[7] H.M. Metwally, R.M. Manglik, Enhanced heat transfer due to curvature-induced lateral vortices in laminar flows in sinusoidal corrugated-plate channels, Int. J. Heat Mass Transfer 47 (2004) 2283–2292.
[8] D.R. Sawyers, M. Sen, H.-C. Chang, Heat transfer enhancement in three-dimensional corrugated channel flow, Int. J. Heat Mass Transfer 41 (1998) 3559–3573.
[9] S. Ray, A.W. Date, Laminar flow and heat transfer through square duct with twisted tape insert, Int. J. Heat Fluid Flow 22 (2001) 460–472.
[10] S. Ray, A.W. Date, Friction and heat transfer characteristics of flow through square duct with twisted tape insert, Int. J. Heat Mass Transfer 46 (2003) 889–902.
[11] A. Murata, S. Mochizuki, Comparison between laminar and turbulent heat transfer in a stationary square duct with transverse or angled rib turbulators, Int. J. Heat Mass Transfer 44 (2001) 1127–1141.
[12] C.E. Kalb, J.D. Seader, Heat and mass transfer phenomena for viscous flow in curved circular tubes, Int. J. Heat Mass Transfer 15 (4) (1972) 801–817.
[13] L. Wang, T. Yang, Bifurcation and stability of forced convection in curved ducts of square cross-section, Int. J. Heat Mass Transfer 47 (2004) 2971–2987.
[14] G. Yang, Z.F. Dong, M.A. Ebadian, Laminar forced convection in a helicoidal pipe with fine pitch, Int. J. Heat Mass Transfer 38 (5) (1995) 853–862.

[15] E. Nobile, F. Pinto, G. Rizzetto, Geometric parameterization and multiobjective shape optimization of convective periodic channels, Numer. Heat Transfer B 50 (2006) 425–453.
[16] N.R. Rosaguti, D.F. Fletcher, B.S. Haynes, Laminar flow and heat transfer in a periodic serpentine channel, Chem. Eng. Technol. 28 (3) (2005) 353–361.
[17] N.R. Rosaguti, D.F. Fletcher, B.S. Haynes, Laminar flow and heat transfer in a periodic serpentine channel with semi-circular cross-section, Int. J. Heat Mass Transfer 49 (17–18) (2006) 2912–2923.
[18] P.E. Geyer, N.R. Rosaguti, D.F. Fletcher, B.S. Haynes, Laminar thermohydraulics of square ducts following a serpentine channel path, Microfluidics Nanofluidics 2 (3) (2006) 195–204.
[19] P.E. Geyer, N.R. Rosaguti, D.F. Fletcher, B.S. Haynes, Laminar flow and heat transfer in periodic serpentine mini-channels, J. Enhanched Heat Transfer 13 (4) (2006) 309–320.
[20] R.K. Shah, A.L. London, Laminar Flow Forced Convection in Ducts: A Source Book for Compact Heat Exchanger Analytical Data, Academic Press, New York, 1978.
[21] N.R. Rosaguti, D.F. Fletcher, B.S. Haynes, General implementation of the H1 boundary condition in CFD simulations of heat transfer in swept passages, Int. J. Heat Mass Transfer 50 (9–10) (2007) 1833–1842.
[22] L.J. Brognaux, R.L. Webb, L.M. Chamra, B.Y. Chung, Single-phase heat transfer in micro-fin tubes, Int. J. Heat Mass Transfer 40 (18) (1997) 4345–4357.